


Quantum bicritical point and phase separation in a frustrated Heisenberg ladder

D. S. Almeida  and R. R. Montenegro-Filho 

Laboratório de Física Teórica e Computacional, Departamento de Física, Universidade Federal de Pernambuco, 50760-901 Recife, Pernambuco, Brazil

 (Received 2 November 2022; revised 18 November 2023; accepted 8 December 2023; published 27 December 2023)

We use the density matrix renormalization group (DMRG) and a hard-core boson map to investigate the quantum phase transitions present in the phase diagram of the frustrated Heisenberg ladder in a magnetic field. The quantum bicritical point is observed at the end of a first-order transition line, which is at the meeting of the two second-order transition lines that bound the fully polarized plateau. The characterization of the bicritical point was made using a hard-core boson mapping of the low-energy excitations from the fully polarized phase and through DMRG by studying the probability density of finding the rung spins in a singlet or a triplet state with zero spin component along the magnetic field. In particular, we give conditions for the exchange couplings for the presence of the first-order transition line and the bicritical point in the phase diagram. Moreover, we unveil the phase-separated states for magnetization values inside the magnetization jump and, in particular, the dependence on the system size of the energy curve as a function of magnetization. Finite-size scaling analysis of the transverse spin correlation functions has been used to estimate the critical points of the Kosterlitz-Thouless transitions from the fractional magnetization plateau $m = 1/2$ to the respective gapless Luttinger liquid phases for some sets of parameters.

DOI: [10.1103/PhysRevB.108.224433](https://doi.org/10.1103/PhysRevB.108.224433)

I. INTRODUCTION

The theory of phase transitions, in the classical [1] and quantum domains [2,3], provides a simple framework to understand the complex phenomenology of systems with many interacting degrees of freedom. Paradigms of strongly correlated states of matter and phase transitions are usually found in models and compounds of magnetic systems. In particular, frustrated systems [4,5] are very fruitful to the physical investigation, presenting features such as the quantum analog to the critical point of water [6], critical end points [7], and quantum bicritical points, as in the heavy-fermion metamagnet YbAgGe [8]. The bicritical point, specifically, is the end point of a first-order transition line, and in its vicinity the system is effectively described by two competing order parameters [9–13]. In a first-order transition, the energy does not present a single global minimum, and phase separation can occur. In a magnetic insulator, this transition appears as a jump in the magnetization curve as a function of the magnetic field.

The spin-1/2 two-leg ladder [14] is gapped, and the ground-state wave function is well described through short-range resonating-valence-bond states [15]. In the presence of a magnetic field [16], the gap closes at a quantum critical point due to the Zeeman effect. The gapless low-energy physics fits that of the Luttinger liquid model [17,18] with a power-law decay of the correlation functions [19]. In fact, the quasi-one-dimensional spin-1/2 ladder compound $(\text{C}_5\text{H}_{12}\text{N})_2\text{CuBr}_4$ has been successfully used to investigate quantum critical points and Luttinger liquid physics [20–22]. Furthermore, other interesting phenomena arise if frustration is added to the model. Special features of frustrated two-leg ladders include their equivalence to spin-1 chains for some exchange patterns and magnetic field ranges [23–25], fractional magnetization

plateaus [26–31] and first-order transitions [25,29,31] (magnetization jumps) in their magnetization curves, spinon and magnon condensation [29], and Kosterlitz-Thouless [32,33] transition points [26–28]. Recently, the unfrustrated Ising ladder with four-spin interactions in a transverse magnetic field showed phase coexistence [34], and the frustrated model was used to understand mode splittings in the ladder compound $(\text{C}_5\text{H}_{12}\text{N})_2\text{CuBr}_4$ [35]. Furthermore, we mention that first-order [36] and Kosterlitz-Thouless transitions [37–40] were identified in one-dimensional ferrimagnetic models.

Here, the density matrix renormalization group (DMRG) [41–43] and a hard-core boson mapping, taking as vacuum the fully polarized state, were used to investigate selected facets of the phase diagram of a two-leg ladder with frustrated couplings along the two diagonals (J_\times) of the plaquettes in a magnetic field. We characterize the quantum bicritical point and associated first-order transition line, particularly the phase-separated states inside the magnetization jump. Moreover, we present a careful numerical estimate of the Kosterlitz-Thouless critical points at which the $m = 1/2$ plateau closes. We mention that the localization of Kosterlitz-Thouless transition points using numerical methods is challenging, since the gap is exponentially small near the critical point [44].

In Sec. II, we show the Hamiltonian of the frustrated ladder, briefly discuss the relevant features of this model, and present the numerical methods used in our calculations. The magnetization curves and a general description of the phase diagram are provided in Sec. III. In Sec. IV, we obtain the single-particle excitations from the fully polarized state through a hard-core boson mapping. The bicritical point is identified in Sec. V by analyzing the transverse spin

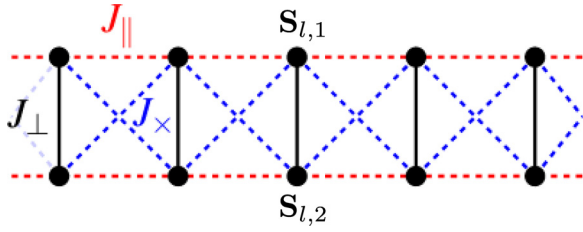


FIG. 1. The frustrated ladder. We consider the phase diagram of the chain as a function of the magnetic field h and J_x , fixing $J_\perp \equiv 1$ and J_\parallel .

correlation functions and the density of dimer excitations in the competing gapless phases. The Kosterlitz-Thouless transition points are estimated through the transverse spin correlation functions in Sec. VI. While we have considered a single set of model parameters in the above sections, in Sec. VII we exhibit the phase diagrams for two other sets to investigate the stability of the observed phases. A summary of the paper is shown in Sec. VIII.

II. MODEL AND METHODS

The Hamiltonian of the frustrated two-leg spin-1/2 ladder with L dimers and open boundary conditions is given by

$$\mathcal{H} = \sum_{l=1}^L \mathbf{S}_{l,1} \cdot \mathbf{S}_{l,2} + J_\parallel \sum_{l=1}^{L-1} (\mathbf{S}_{l,1} \cdot \mathbf{S}_{l+1,1} + \mathbf{S}_{l,2} \cdot \mathbf{S}_{l+1,2}) + J_x \sum_{l=1}^{L-1} (\mathbf{S}_{l,1} \cdot \mathbf{S}_{l+1,2} + \mathbf{S}_{l+1,1} \cdot \mathbf{S}_{l,2}) - hS^z \quad (1)$$

and is schematically illustrated in Fig. 1. We consider the phase diagram of the chain as a function of J_x and the magnetic field h for fixed values of the exchange couplings on the rungs, $J_\perp \equiv 1$, and along the legs, J_\parallel . The direction of the external magnetic field h is defined as the z direction, while $S^z = \sum_l S_l^z = \sum_l (S_{l,1}^z + S_{l,2}^z)$ is the z component of the total spin and $g\mu_B \equiv 1$. We notice, also, that the ladder is symmetric under the exchange of J_x and J_\parallel , and of the label of the spins in odd (or even) dimers.

In the regime $J_\perp \gg (J_\parallel, J_x)$ and $h > 0$, the ladder has each dimer in a $S_l^z = 1$ triplet or in a singlet [26,29,30]. In this case, the Hamiltonian can be mapped onto [26] the XXZ Heisenberg model or the model of interacting spinless fermions in a linear chain. The magnetization per dimer m as a function of h exhibits plateaus at $m = 0$ and $m = 1$ and a fractional plateau at $m = 1/2$ for some combinations of the exchange couplings. In particular, Kosterlitz-Thouless transitions are predicted [26] within this approximation. Furthermore, the presence of magnetization jumps was observed with DMRG [29,31] and for a range of values of J_x for $J_x = J_\parallel$ using DMRG and Maxwell construction [25]. Moreover, the phase diagram for $h = 0$ shows a rung-singlet phase for the J_\perp -dominant regime and a rung-triplet phase (Haldane phase) in the other regimes. A detailed discussion of the $h = 0$ case can be found in Ref. [45].

We used the DMRG and exact diagonalization numerical methods to calculate the magnetization curves and spin

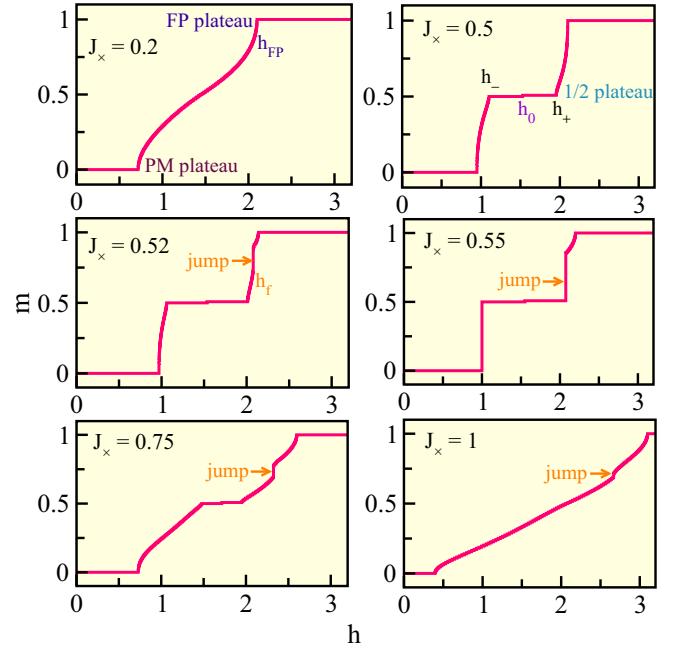


FIG. 2. Magnetization per dimer $m = \langle S^z \rangle / L$ vs magnetic field h for a ladder with $L = 128$ dimers and $J_\parallel = 0.55$. The quantum paramagnetic (PM), 1/2, and fully polarized (FP) plateaus are indicated, as well as the critical magnetic fields h_{PM} , h_- , h_+ , and h_{FP} . We denote by h_r the magnetic field at which the magnetization jump occurs. At the field h_0 , the 1/2 plateau splits into two steps in the finite-size system with open boundary conditions.

correlations of finite-size systems. In the case of DMRG, we used the codes provided by the Algorithms and Libraries for Physics Simulations (ALPS) project [46] and the ITENSOR library [47], beyond our code. In the DMRG simulations, the maximum number of states kept per block, or bond dimension in the case of the tensor code, was 1355, and we have considered chains with open boundaries. The typical discarded weight was less than 1×10^{-10} , while the maximum discarded weight was $\sim 1 \times 10^{-8}$. We also applied a hard-core boson mapping to examine the single-particle excitations from the fully polarized state.

III. MAGNETIZATION CURVES AND PHASE DIAGRAM

We present in Fig. 2 the typical features of the magnetization per dimer m as a function of h as we change J_x keeping $J_\parallel (= 0.55)$ fixed. For a finite-size system, $m(h) = \langle S^z \rangle / L$ have finite-size steps of width $\Delta h(S^z) = h_{S^z+} - h_{S^z-}$ at a given value of S^z , with $h_{S^z\pm} = \pm [E(S^z \pm 1) - E(S^z)]$ being the extreme points of these steps, where $E(S^z)$ is the total energy at a given value of S^z . Magnetization plateaus in the thermodynamic limit are characterized by $\Delta h(S^z) \neq 0$ as $L \rightarrow \infty$.

The Oshikawa-Yamanaka-Affleck argument [48] states that a magnetization plateau can appear at the magnetization m if

$$(S_u - m_u) = \text{integer}, \quad (2)$$

where S_u is the maximum total spin and m_u is the magnetization in the unit cell of the ground-state wave function. In our case, the unit period of the Hamiltonian has two spin-1/2 sites. Thus magnetization plateaus that do not spontaneously break translation symmetry can occur at $m = 0$, the paramagnetic (PM) plateau, and at $m = m_s = 1$, the fully polarized (FP) plateau. For any value of J_\times , these two magnetization plateaus are observed in Fig. 2. Their critical fields are defined as h_{FP} for the FP plateau and h_{PM} for the PM plateau. For moderate values of J_\times , a magnetization plateau appears at 1/2 of the saturation magnetization. In this case, the ground state has a doubled unit cell with four spin-1/2 sites. The critical fields at the extreme of the 1/2 plateau are indicated by h_- and h_+ . In a finite-size chain with open boundary conditions, this plateau is made of two steps joined at $h = h_0$. These two steps consist in domain walls [29], and we briefly discuss them in Sec. VI. Between the thermodynamic-limit magnetization plateaus, there are gapless Luttinger liquid (LL) phases [16] with critical power-law transverse spin correlation functions with the asymptotic form

$$\Gamma(r) \sim \frac{1}{r^{1/2K}}, \quad (3)$$

where K is the Luttinger liquid exponent and r is the distance between spins along the chain. Furthermore, there is a magnetization jump at $h = h_f$ for $J_\times > 0.5$.

In Fig. 3, we show our estimated phase diagram h versus J_\times for the frustrated ladder with $J_\parallel = 0.55$. There, we highlight the magnetization m , given by the color code, for a system with $L = 128$, and the thermodynamic-limit boundary lines of the magnetization plateaus. For fixed values of J_\times , there are typically second-order transitions at the extremes of the plateau: h_{FP} , h_- , h_+ , and h_{PM} . As the second-order transition point is approached from the gapless side of the transition [49], $K \rightarrow 1$ at the boundaries of the plateaus with the same periodicity of the Hamiltonian (PM plateau and FP plateau), while $K \rightarrow 1/4$ at the boundaries of the 1/2 plateau. However, at some points, the transitions in the plateau extremes are of the first-order kind: for $J_\times = 0.55 = J_\parallel$, at the PM-plateau and 1/2-plateau transition lines. Magnetization curves exhibit magnetization jumps in the first-order transition line h_f . In particular, this line ends at a bicritical point at $J_\times = 0.5$, which is the endpoint of the two second-order transition lines that bound the FP plateau. For fixed m , the 1/2 plateau closes at two points through transitions of Kosterlitz-Thouless (KT) type: $J_{\times,KT_1} = 0.255 \pm 0.005$ and $h_{KT_1} = 1.467 \pm 0.002$; $J_{\times,KT_2} = 0.935 \pm 0.005$ and $h_{KT_2} = 1.98 \pm 0.01$. In these cases, $K \rightarrow 1/2$ as the transition points are approached from its gapless side.

In the following, we discuss some features of the phase diagram shown in Fig. 3. In particular, we estimate the first-order transition line for $J_\parallel = 0.55$ and characterize the bicritical transition point at the end of this line. Moreover, we use a confident numerical methodology to estimate the exact critical values of h and J_\times for the KT transitions. Furthermore, we exhibit phase diagrams for $J_\parallel = 0.2$ and 0.8 to explore the stability of the observed phases and transition lines under changes in J_\parallel .

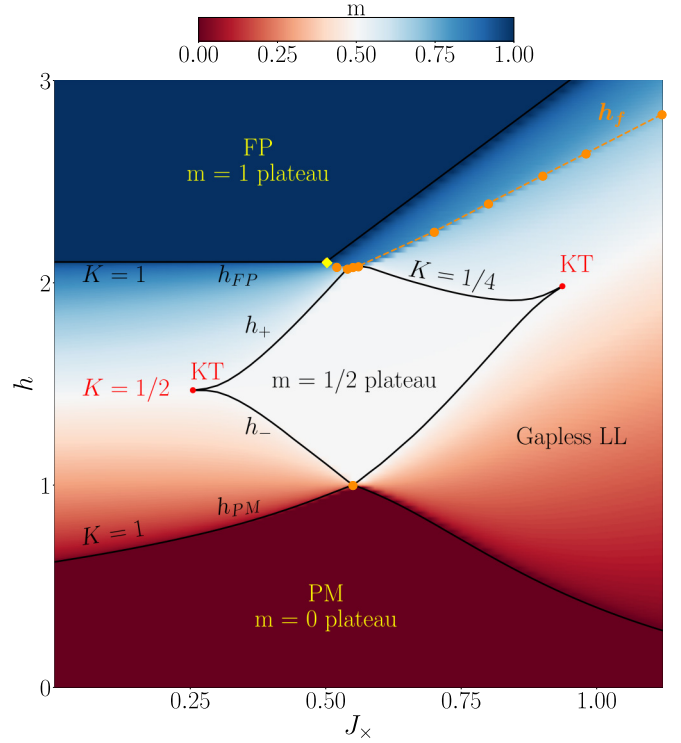


FIG. 3. DMRG results for the thermodynamic-limit magnetic field h vs frustration J_\times phase diagram for $J_\parallel = 0.55$. The color code gives the magnetization for a finite-size chain with $L = 128$. The gapped fully polarized (FP), 1/2, and paramagnetic (PM) plateaus are bounded by the lines h_{FP} , h_+ , h_- , and h_{PM} , respectively. The intermediate regions between plateaus are gapless Luttinger liquid (LL) phases. We indicate the limiting value of the Luttinger liquid parameter K as the second-order transition points are approached from the gapless phases. Along the first-order transition line h_f , the magnetization curve m vs h exhibits a jump. The line h_f starts at a bicritical point (yellow diamond) in the h_{FP} line. We mark with orange circles the two first-order transition points on the line $J_\times = J_\parallel$. The $m = 1/2$ plateau closes at the Kosterlitz-Thouless (KT) transition points (red circles), for which $K \rightarrow 1/2$ on the gapless side of the transition.

IV. HARD-CORE BOSON MAPPING

The critical transition line from the fully polarized state, h_{FP} , can be precisely determined by mapping the spin variables to hard-core boson operators [50]:

$$\begin{aligned} S_{l,i}^z &= \frac{1}{2} - a_{l,i}^\dagger a_{l,i} = \frac{1}{2} - n_{l,i}, \\ S_{l,i}^+ &= a_{l,i}, \quad S_{l,i}^- = a_{l,i}^\dagger. \end{aligned}$$

To preserve the momentum angular commutation relations, $[S_{l,i}^+, S_{m,j}^-] = 2\delta_{lm}\delta_{ij}S_{l,i}^z$ and $[S_{m,j}^z, S_{l,i}^\pm] = \pm\delta_{lm}\delta_{ij}S_{l,i}^\pm$, with $S^\pm = S^x \pm iS^y$; besides the constraints $S_{l,i}^+ S_{l,i}^- + S_{l,i}^- S_{l,i}^+ = 1$ and $(S_{l,i}^+)^2 = (S_{l,i}^-)^2 = 0$ specific to spin-1/2 operators, the commutation relation

$$[a_{l,i}, a_{m,j}^\dagger] = \delta_{lm}\delta_{ij}(1 - 2n_{l,i}) \quad (4)$$

must be satisfied by the bosonic operators, in addition to $(a_{l,i})^2 = (a_{l,i}^\dagger)^2 = 0$.

In the bosonic variables, the Hamiltonian (1) is written as

$$\begin{aligned}
 H^{(\text{free hc})} = & \left(-\frac{1}{2} + J_{\parallel} + J_{\times} \right) N + hN \\
 & + \frac{1}{2} \sum_l (a_{l,1}^{\dagger} a_{l,2} + a_{l,2}^{\dagger} a_{l,1}) \\
 & + \frac{J_{\parallel}}{2} \sum_l \sum_{i=1}^2 (a_{l,i}^{\dagger} a_{l+1,i} + a_{l+1,i}^{\dagger} a_{l,i}) \\
 & + \frac{J_{\times}}{2} \sum_l (a_{l,1}^{\dagger} a_{l+1,2} + a_{l,2}^{\dagger} a_{l+1,1} + \text{H.c.}), \quad (5)
 \end{aligned}$$

where $N = \sum_l (n_{l,1} + n_{l,2})$ is the total number of bosons and we have discarded interaction and constant terms. The Hamiltonian (5) can be straightforwardly diagonalized if we use odd and even combinations of $a_{l,1}$ and $a_{l,2}$:

$$\begin{aligned}
 s_l^{\dagger} &= \frac{1}{\sqrt{2}} (a_{l,1}^{\dagger} - a_{l,2}^{\dagger}), \\
 t_{0,l}^{\dagger} &= \frac{1}{\sqrt{2}} (a_{l,1}^{\dagger} + a_{l,2}^{\dagger}). \quad (6)
 \end{aligned}$$

When applied to the fully polarized state |FP>, s_l^{\dagger} creates a singlet state between the two sites at the dimer l ,

$$s_l^{\dagger} |\text{FP}\rangle = \frac{1}{\sqrt{2}} (|\downarrow\uparrow\rangle_l - |\uparrow\downarrow\rangle_l) = |s_l\rangle, \quad (7)$$

while $t_{0,l}^{\dagger}$ creates a triplet state with total spin component $S_l^z = 0$ at the dimer l ,

$$t_{0,l}^{\dagger} |\text{FP}\rangle = \frac{1}{\sqrt{2}} (|\downarrow\uparrow\rangle_l + |\uparrow\downarrow\rangle_l) = |t_{0,l}\rangle. \quad (8)$$

Writing the Hamiltonian (5) in the variables (6) and Fourier transforming, we arrive at the diagonal Hamiltonian:

$$H^{(\text{free hc})} = \sum_q \varepsilon_q^s s_q^{\dagger} s_q + \sum_q \varepsilon_q^t t_{0,q}^{\dagger} t_{0,q}, \quad (9)$$

where the dispersion relations are given by

$$\varepsilon_q^t = -(J_{\parallel} + J_{\times}) + (J_{\parallel} + J_{\times}) \cos(q) + h, \quad (10)$$

$$\varepsilon_q^s = -1 - (J_{\parallel} + J_{\times}) + (J_{\parallel} - J_{\times}) \cos(q) + h \quad (11)$$

and are shown in Fig. 4 for specific values of J_{\times} and h , with $J_{\parallel} = 0.55$.

The magnetic fields used in Fig. 4 are the critical fields h_{FP} for the respective values of J_{\times} and are determined as follows. Since the lowest energy of the triplet band is

$$\varepsilon_{\min}^t = \varepsilon_{q=\pi}^t = -2(J_{\parallel} + J_{\times}) + h, \quad (12)$$

the triplet component condenses at a field

$$h_c^t = 2J_{\parallel} + 2J_{\times}. \quad (13)$$

On the other hand, the lowest energy of the singlet band is

$$\varepsilon_{\min}^s = \varepsilon_{q=\pi}^s = -1 - 2J_{\parallel} + h \quad \text{for } J_{\times} < J_{\parallel}, \quad (14)$$

$$\varepsilon_{\min}^s = \varepsilon_{q=0}^s = -1 - 2J_{\times} + h \quad \text{for } J_{\times} > J_{\parallel}. \quad (15)$$

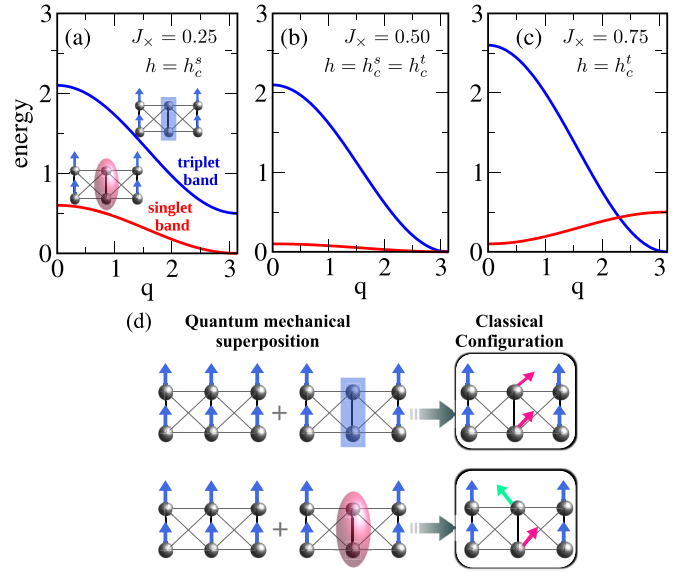


FIG. 4. (a)–(d) Free singlet and triplet hard-core bosons bands for $J_{\parallel} = 0.55$ and the indicated values of J_{\times} and magnetic field h . The critical fields $h_c^s = 1 + 2J_{\parallel}$ and $h_c^t = 1 + 2J_{\times}$. In (a) and (d), we illustrate with a blue box a triplet state $|t_{0,l}\rangle = \frac{1}{\sqrt{2}}(|\downarrow\uparrow\rangle + |\uparrow\downarrow\rangle)$ and with a red ellipse a singlet state $|s_l\rangle = \frac{1}{\sqrt{2}}(|\downarrow\uparrow\rangle - |\uparrow\downarrow\rangle)$ between the spins of a dimer.

Thus the singlet component condenses at

$$h_c^s = 1 + 2J_{\parallel} \quad \text{for } J_{\times} < J_{\parallel}, \quad (16)$$

$$h_c^s = 1 + 2J_{\times} \quad \text{for } J_{\times} > J_{\parallel}. \quad (17)$$

We determine the critical field h_{FP} for given values of J_{\times} and J_{\parallel} by finding the minimum energy between those in (12), (14), and (15). First, we draw the line $J_{\times} = J_{\parallel}$ in Fig. 5, since the minimum of the singlet band is given by Eq. (16) for $J_{\times} < J_{\parallel}$ and according to Eq. (17) for $J_{\times} > J_{\parallel}$. In sector $J_{\times} < J_{\parallel}$, the minimum energy of the singlet band crosses the minimum of the triplet one at $J_{\times} = 1/2$, as indicated by a comparison of Eqs. (12) and (14). In the sector $J_{\times} > J_{\parallel}$, Eqs. (12) and (15) show that the crossing occurs at $J_{\parallel} = 1/2$. For example, consider the phase diagram of Fig. 3. Fixing J_{\parallel} at 0.55 and

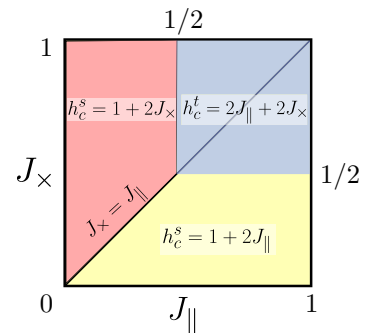


FIG. 5. Expressions for the critical fully polarized field h_{FP} as a function of J_{\times} and J_{\parallel} , as obtained by comparing the minimum energy of the single-particle triplet and singlet bands: Eqs. (12), (14), and (15).

changing J_\times , we have $h_{\text{FP}} = h_c^s = 2.1$ for $J_\times < 0.5$ and $h_{\text{FP}} = h_c^t = 2.1 + 2J_\times$ for $J_\times > 0.5$. From Fig. 5, we also note that the crossing between the singlet and triplet bands is absent for $J_\parallel < 1/2$.

V. MAGNETIC ORDER IN THE HIGH-FIELD REGIME: BICRITICAL POINT, FIRST-ORDER TRANSITION LINE, AND PHASE SEPARATION

Here, we show the average triplet and singlet components, as well as the correlation functions calculated with DMRG for $J_\perp = 0.55$. This section mainly aims at the region $m > 1/2$.

The average probability density of singlets at the dimer l can be written as

$$\begin{aligned} \langle n_l^s \rangle &= \langle s_l^\dagger s_l \rangle = \frac{1}{4} - \langle \mathbf{S}_{l,1} \cdot \mathbf{S}_{l,2} \rangle + \langle n_{l,1} n_{l,2} \rangle \\ &\approx \frac{1}{4} - \langle \mathbf{S}_{l,1} \cdot \mathbf{S}_{l,2} \rangle, \end{aligned} \quad (18)$$

while the average probability density of triplets $|t_0\rangle$ at the dimer l can be written as

$$\begin{aligned} \langle n_l^{t_0} \rangle &= \langle t_{0,l}^\dagger t_{0,l} \rangle = \frac{3}{4} - \langle S_l^z \rangle + \langle \mathbf{S}_{l,1} \cdot \mathbf{S}_{l,2} \rangle - \langle n_{l,1} n_{l,2} \rangle \\ &\approx \frac{3}{4} - \langle S_l^z \rangle + \langle \mathbf{S}_{l,1} \cdot \mathbf{S}_{l,2} \rangle, \end{aligned} \quad (19)$$

where $S_l^z = S_{l,1}^z + S_{l,2}^z$. In both expressions, we have discarded the term $\langle n_{l,1} n_{l,2} \rangle$, which is nonzero if the dimer is in the triplet state $|\downarrow\downarrow\rangle$, which has a low probability of occurrence.

We investigate the total probability of occurrence of dimer singlets and triplets through the two probability density parameters $\langle n_s \rangle$ and $\langle n_{t_0} \rangle$:

$$\begin{aligned} \langle n_s \rangle &= \frac{1}{L} \sum \langle n_l^s \rangle, \\ \langle n_{t_0} \rangle &= \frac{1}{L} \sum \langle n_l^{t_0} \rangle. \end{aligned} \quad (20)$$

In Fig. 6, we show the behavior of $\langle n_s \rangle$ and $\langle n_{t_0} \rangle$ for $J_\times = 0.75$ ($J_\times = 0.4$ in the inset), for $0.5 < m < 1.0$. In particular, we notice that the data cross the first-order transition line h_f of the phase diagram (shown in Fig. 3) for $J_\times = 0.75$. For $m_f < m < 1$, with $m_f \approx 0.78$, we have $\langle n_s \rangle = 0$ and $\langle n_{t_0} \rangle \neq 0$, while $\langle n_s \rangle \neq 0$ and $\langle n_{t_0} \rangle = 0$ for $0.5 < m < 0.70$. There is also a range of magnetization values, $\Delta m = m_f - m_i = 0.78 - 0.70 = 0.08$, for which phase coexistence is observed in spatially separated regions, with $\langle n_{t_0} \rangle \neq 0$ and $\langle n_s \rangle \neq 0$. For $J_\times = 0.4$, in the inset of Fig. 6, the first-order transition line is not crossed (see Fig. 3), and we have $\langle n_{t_0} \rangle = 0$ and $\langle n_s \rangle \neq 0$ for $0.5 < m < 1$. For $m < 0.5$, there is the coexistence of both components along the total extension of the ladder, such that any dimer is in a coherent superposition of both components.

The quasi-long-range magnetic order in the high-field regime can be described by considering $\langle n_s \rangle$, $\langle n_{t_0} \rangle$, and the transverse spin correlation functions. We consider two types of transverse spin correlation functions: the first between spins along the same leg $\Gamma_{11}(r) = \Gamma_{22}(r)$, and the other between spins in different legs $\Gamma_{12}(r) = \Gamma_{21}(r)$. In both cases, to reduce boundary effects, we average $\langle (\dots)_{|m-l|=r} \rangle$ the transverse spin correlation $\langle S_{l,i}^+ S_{m,j}^- + S_{l,i}^- S_{m,j}^+ \rangle$ over all pairs of dimers l and m separated by the same distance r , such that

$$\Gamma_{ij}(r) = \frac{1}{2} \langle \langle S_{l,i}^+ S_{m,j}^- + S_{l,i}^- S_{m,j}^+ \rangle \rangle_{|m-l|=r}. \quad (21)$$

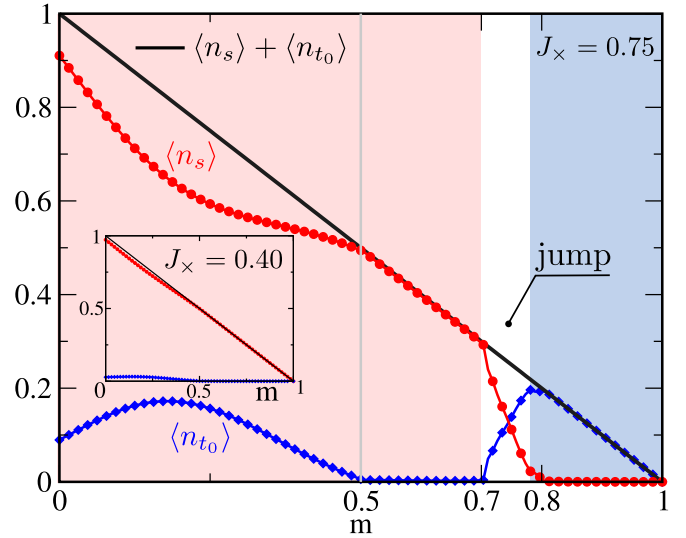


FIG. 6. DMRG results for the average density of singlets $\langle n_s \rangle$ and triplets $\langle n_{t_0} \rangle$ as a function of the magnetization m for a system of size $L = 128$, with $J_\parallel = 0.55$ and $J_\times = 0.75$. The magnetization states inside the magnetization jump are observed for $0.7 \lesssim m \lesssim 0.78$. Inset: the same parameters as in the main figure, except that $J_\times = 0.40$.

We sketch in Fig. 7 the short-range (power-law decaying) magnetic orders in the phases, named phases I, I', and II, which are competing in the high-field regime. The values of $\langle n_s \rangle$ and $\langle n_{t_0} \rangle$ in each phase are indicated, and we present the behavior of $\Gamma_{11}(r)$ and $\Gamma_{12}(r)$ for representative points in these phases.

First, we discuss the presence of a bicritical point [1,9,10] at $J_\times = 0.5$ and $h = 2.1$. At this point, the two critical phases become identical to the disordered fully polarized phase. The bicritical point can thus be characterized by probability densities $\langle n_s \rangle$ and $\langle n_{t_0} \rangle$, as defined in Eqs. (18) and (19), respectively. The disordered phase, the fully polarized magnetization, is gapped with $\langle n_s \rangle = 0$ and $\langle n_{t_0} \rangle = 0$. For $J_\times < 0.5$, as the field is reduced, the singlet component condenses, and the average probability density $\langle n_s \rangle \neq 0$ in phase I, with $\langle n_{t_0} \rangle = 0$. For $J_\times > 0.5$, as the field is reduced, the component $|t_0\rangle$ condenses, and thus we find an average probability density $\langle n_{t_0} \rangle \neq 0$ in phase II, with $\langle n_s \rangle = 0$. In fact, in phase II, the frustrated ladder is effectively described by a spin-1 chain in a magnetic field. We mention that in the symmetrical case, $J_\times = J_\parallel$, the effective description of the frustrated ladder by spin-1 chains was revealed for $h = 0$ in Ref. [23] and for $h \neq 0$ in Ref. [25]. Furthermore, the equivalence between the low-energy behavior of frustrated ladders and spin-1 chains was also observed for other frustration patterns and zero magnetic field [24].

The transition from phase II, with $\langle n_{t_0} \rangle \neq 0$ and $\langle n_s \rangle = 0$, to phase I or phase I', both with $\langle n_{t_0} \rangle = 0$ and $\langle n_s \rangle \neq 0$, is of first order and is indicated by the transition line h_f . Furthermore, near $J_\times = J_\parallel = 0.55$, the transition from the plateau $m = 1/2$ to phase II is also of the first-order kind.

We notice that the line for the condensation of the singlet component h_c^s , Eqs. (16) and (17), from the free hard-core boson model in (5), also shown in Fig. 7, has a trend that resembles the line h_f from the DMRG data. In particular, for

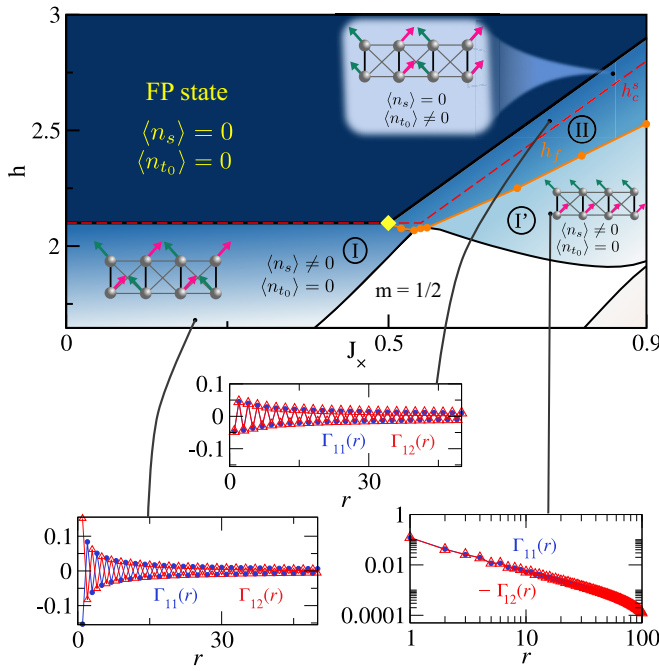


FIG. 7. Short-range magnetic ordering near the fully polarized (FP) magnetization plateau as indicated by the transverse spin correlation functions along one of the legs, $\Gamma_{11}(r)$, and between spins in distinct legs, $\Gamma_{12}(r)$, shown in the bottom panels. In phases I and I' , the average density of singlets $\langle n_s \rangle \neq 0$ and the average density of triplets $|t_0\rangle$ is $\langle n_{t_0} \rangle \approx 0$, while in phase II $\langle n_s \rangle \approx 0$ and $\langle n_{t_0} \rangle \neq 0$. We indicate the bicritical point (yellow diamond) at $J_x = 0.5$ and $h = 1 + 2J_{\parallel} = 2.1$. The dashed line h_c^s is the critical line for the condensation of the singlet component in the noninteracting model, while h_f is the thermodynamic-limit first-order transition line from DMRG.

$J_x < J_{\parallel}$, $h_c^s = 1 + 2J_{\parallel} = 2.1$ is constant, and $h_c^s = 1 + 2J_x = 2.1$ for $J_x > J_{\parallel}$, having an upward slope. Compared with it, the DMRG results for h_f show that the interactions have introduced an average downward slope for the line in the region $J_x > J_{\parallel}$ and also for the horizontal line in the region $0.5 < J_x < J_{\parallel}$.

The phases I, I' , and II are gapless phases in which dimers are predominantly found in a coherent superposition of triplets $|\uparrow\uparrow\rangle$ and singlets (phases I and I') or triplets $|t_0\rangle$ (phase II). Thus the dimer spins present the classical orientations depicted in Fig. 4(d). The canted orientation of the dimer spins and the competition between J_x and J_{\parallel} explain the quasi-long-range magnetic order of phases I and I' . For $J_x < J_{\parallel}$ there is a quasi-long-range transverse antiferromagnetic order between spins in the same leg, while for $J_x > J_{\parallel}$ this order is observed between spins of distinct legs. Phases I and I' meet at the gapped $m = 1/2$ magnetization, the fully frustrated point $J_x = J_{\parallel} = 0.55$, for which the singlet and triplet $|\uparrow\uparrow\rangle$ components are localized, as will be discussed in the next section. In contrast to phases I and I' , in phase II, there is no competition between J_x and J_{\parallel} , since, in this case, the coherent superposition between the triplet components $|t_0\rangle$ and $|\uparrow\uparrow\rangle$ satisfies both couplings. In this case, the transverse spin correlation functions present an antiferromagnetic quasi-long-range order between spins along the legs and between spins in distinct legs.

Phase separation

Along the first-order transition line $h = h_f(J_x)$ shown in Figs. 3 and 7, we expect phase coexistence between phase II and phases I or I' . Around $h = h_f(J_x)$ the competition occurs between a singlet-rich phase (phases I or I') and a phase rich in triplets $|t_0\rangle$ (phase II). In the thermodynamic limit, precisely at $h = h_f$, the energy curve as a function of m has a flat region, with degenerate magnetization states in the range $m_i^{(\text{jump})} < m < m_f^{(\text{jump})}$, where $m_i^{(\text{jump})}$ and $m_f^{(\text{jump})}$ are the extreme magnetizations of the jump. At $m = m_i^{(\text{jump})}$ (phases I or I'), we should have $\langle n_s \rangle \neq 0$ and $\langle n_{t_0} \rangle = 0$, while at $m = m_f^{(\text{jump})}$ (phase II), $\langle n_s \rangle = 0$ and $\langle n_{t_0} \rangle \neq 0$; see Figs. 7 and 2. In the flat portion of the energy curve, $m_i^{(\text{jump})} < m < m_f^{(\text{jump})}$, the states exhibit spatial separation of phases I or I' (singlet rich) and phase II (triplet rich). Thus, to complete the whole physical picture associated with the first-order transition line and the bicritical point, we investigate the distribution of $\langle n_s \rangle$ and $\langle n_{t_0} \rangle$ along the ladder near the transition.

We show the energy per dimer $E_{h=h_t(L)}/L$ as a function of m at the respective value of the transition field $h = h_t(L)$ in Fig. 8(a). The curves are translated by the respective value of the energy minimum, $E_{h=h_t(L),\text{min}}/L$. In the inset of this figure, we have put the finite-size magnetization curves as a reference. In particular, we notice the presence of two minima separated from each other by a region of unstable states in finite-size systems.

In Fig. 8(b), we present the magnetization, singlet, and triplet $|t_0\rangle$ distributions along the chain. Data show that at minimum $m = m_i^{(\text{jump})}$, the ladder is in the singlet-rich phase I' , while at minimum $m = m_f^{(\text{jump})}$ its bulk is in the triplet-rich phase II. Furthermore, as shown in the central panel of Fig. 8(b), the states in the straight line portion of the energy curves exhibit phase separation.

A finite-size scaling analysis of the angular coefficient of the straight line portion in the energy curves of Fig. 8(a), the region highlighted, shows that the thermodynamic-limit straight line is horizontal, joining the two single-phase states, and the energy density as a function of m is an equilibrium curve. Furthermore, the size dependence of the energy curves in the linear regime implies that the energy density of phase I' differs from the energy density of phase II by a term a/L , where a is a constant. Since this difference is in the size L of the whole system, we attribute it to the interface between the two coexisting states.

In Fig. 9, we present the phase diagram m versus J_x for $0.5 \leq m \leq 1$ and $0.5 \leq J_x \leq 1.12$ for a ladder with 128 dimers. We are interested in observing the magnetization region bounded by $m_i^{(\text{jump})}$ and $m_f^{(\text{jump})}$ as a function of J_x , particularly to show that $m_i^{(\text{jump})} \rightarrow m_f^{(\text{jump})} \rightarrow 1$ as $J_x \rightarrow 0.5$, the quantum bicritical point. We also show singlet and triplet distributions of $|t_0\rangle$, $\langle n_s^s \rangle$ and $\langle n_{t_0}^t \rangle$, along a 128-dimer ladder for $(J_x = 0.52, m \approx 0.8)$ and $(J_x = 0.50, m \approx 0.7)$. The region of phase separation is limited by the bicritical point, $(J_x = 0.50, m = 1)$, on the left, and we could identify not a jump, but a discontinuity in the slope of the magnetization curve at $J_x \gtrsim 1.1$ on the right. For magnetizations $m_i^{(\text{jump})} < m < m_f^{(\text{jump})}$, the gapless phase II

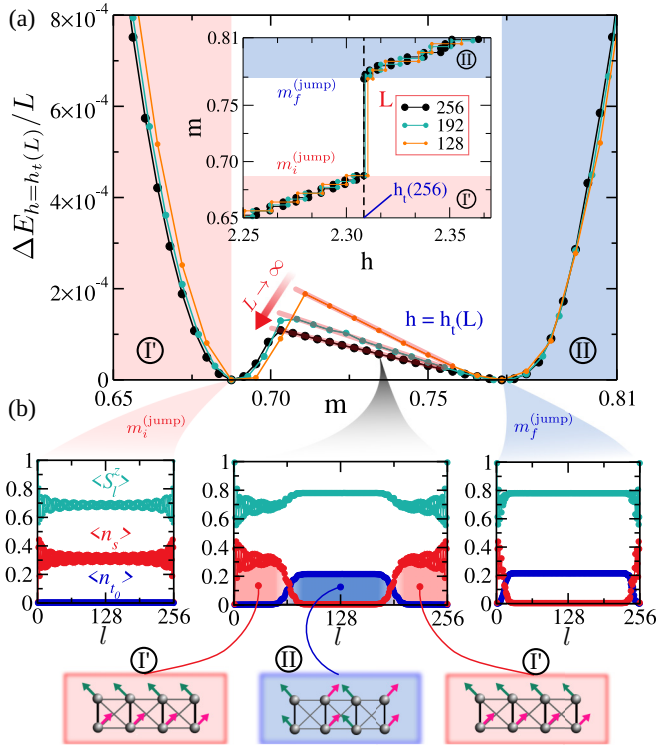


FIG. 8. (a) The difference between the energy per dimer ($E_{h=h_t(L)}/L$) and its minimum: $\Delta E_{h=h_t(L)}/L = (E_{h=h_t(L)} - E_{h=h_t(L),\text{min}})/L$, as a function of the magnetization m near the magnetization jump for $J_\times = 0.74$, $J_\parallel = 0.55$, and magnetic field $h = h_t(L)$, where $h_t(L)$ is the value of h at which the jump is observed in systems of size $L = 128, 192, 256$. The inset displays m as a function of h for the magnetization range shown in the main figure. We indicate the lower, $m_i^{(\text{jump})}$, and the upper, $m_f^{(\text{jump})}$, values of the magnetization that limit the magnetization jump. (b) The magnetization distribution, $\langle S_i^z \rangle$, and average probability densities of singlet, $\langle n_s \rangle$, and triplet $|t_0\rangle$, $\langle n_t \rangle$, states along a chain of size $L = 256$ for $m = m_i^{(\text{jump})}$, $m_f^{(\text{jump})}$, and an intermediate value of m ($= 188/256$), as indicated in (a). In the central panel, we illustrate the phases in each region of the chain (see also Fig. 7).

coexists with the gapless phase I for $0.5 < J_\times < 0.55 = J_\parallel$ and with the gapless phase I' for $J_\times > 0.55$. On the other hand, phase II coexists with the gapped $m = 1/2$ state at $J_\times = J_\parallel$ and $m_i^{(\text{jump})} < m < m_f^{(\text{jump})}$.

In particular, we discuss a technical difficulty in obtaining the distributions for $J_\times = J_\parallel = 0.55$. In this case, the gapless phase II coexists with the gapped $m = 0.5$ state, and the renormalization procedure becomes more complex. For $J_\times = J_\parallel$, the Hamiltonian is invariant under the exchange of spin variables $\mathbf{S}_{l,1}$ and $\mathbf{S}_{l,2}$ in the same dimer. Therefore each dimer has constant parity. Since the Hamiltonian cannot connect different parity sectors, the parity of the dimers is fixed in the growth stage of the renormalization procedure and cannot change in the sweeping stage of the DMRG. Also, we notice that the singlet band (11) becomes flat at $J_\times = J_\parallel$, implying that the interaction controls the physics at this point. Due to these issues, if we run the DMRG procedure targeting only the desired value of m , the algorithm converges to a higher energy state presenting a phase-separated state with clusters of variable size of phase II separated by clusters of

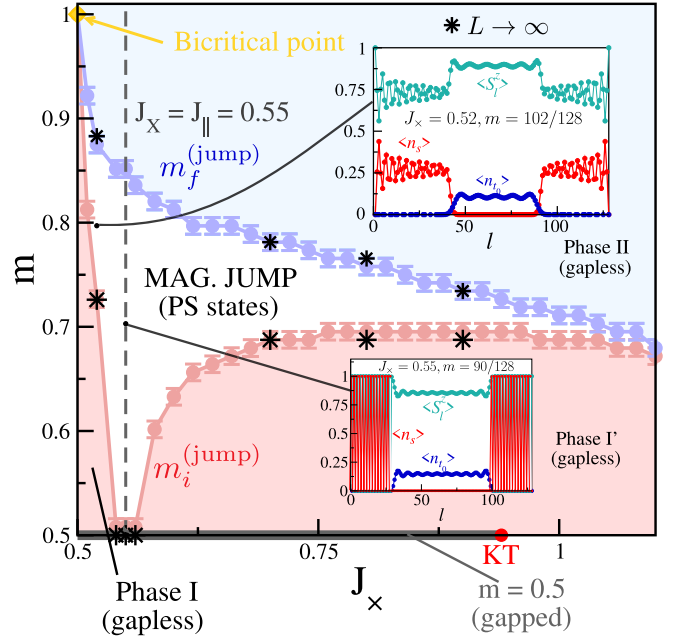


FIG. 9. DMRG results for the lower, $m_i^{(\text{jump})}$, and upper, $m_f^{(\text{jump})}$, magnetization values bounding the magnetization jump (mag. jump) as a function of J_\times for $J_\parallel = 0.55$: red and blue circles, $L = 128$; black asterisks, $L \rightarrow \infty$. Error bars are defined as the minimum Δm value for the system size: $\Delta m = 1/128$. Phases I, I', and II are those sketched in Fig. 7. The bicritical point at $J_\times = 0.5$ and $m = 1$ ($h = 2.1$ in Fig. 7) and the Kosterlitz-Thouless (KT) point are also indicated. Insets: probability density of singlets ($\langle n_s \rangle$) and triplets $|t_0\rangle$ ($\langle n_t \rangle$) along the chain for $J_\times = 0.52$ and $m = 102/128$ (upper inset) and for $J_\times = 0.55$ and $m = 90/128$ (lower inset). PS states, phase-separated states.

the $m = 1/2$ state. However, the lowest energy state shown in Fig. 9 has only two domains and can be reached by running the DMRG procedure twice. First, we target the final value of m , and at the end of the run, we estimate the total size l_0 of the $m = 1/2$ phase as the sum of the sizes of the clusters of this phase. In the second run, we target the sector $m = 1/2$ in the growth stage until the chain has a size equal to l_0 , and after that we target the desired value of m . At this time, the wave function converges to the phase-separated state shown in Fig. 9, which has lower energy than the one obtained in the first run.

VI. $m = 1/2$ MAGNETIZATION PLATEAU AND THE KOSTERLITZ-THOULESS TRANSITION POINTS

The magnetization plateau state $m = 1/2$ can be better qualitatively understood from the $J_\times = J_\parallel$ line [25,29]. Because all dimers have a fixed parity, they cannot be found in a coherent superposition of singlet and triplet states. The ground-state wave function has a singlet alternating with a triplet $|\uparrow\uparrow\rangle$ along the lattice due to the repulsion energy between two triplets if they are in neighbor dimers. In a finite chain with periodic boundary conditions (PBCs) [29], there are two degenerate states, as illustrated in Fig. 10(a). However, for a finite chain with open boundary conditions (OBCs), the lowest energy states have triplets $|\uparrow\uparrow\rangle$ at the edges of the

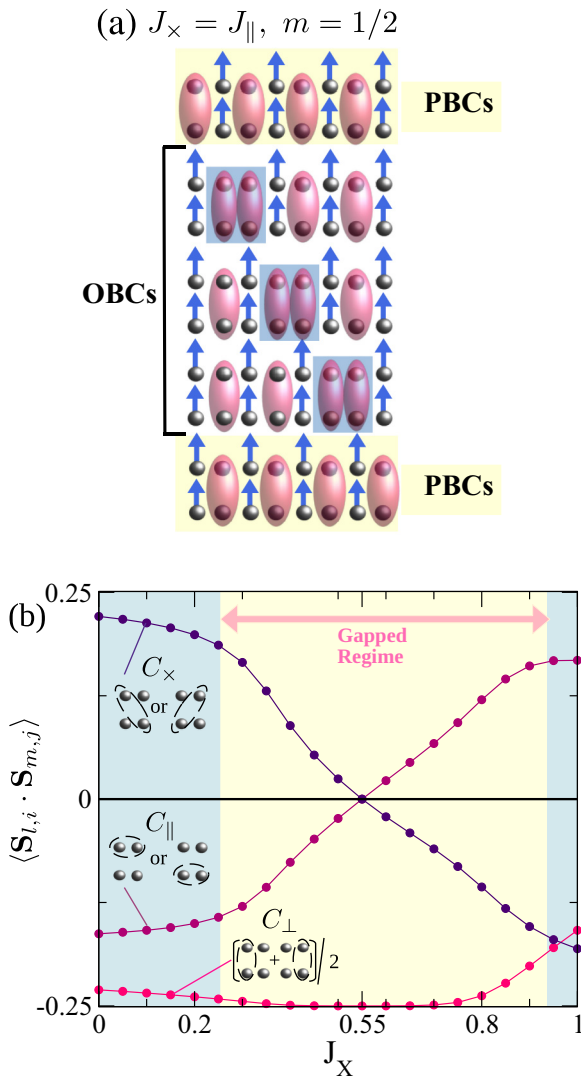


FIG. 10. (a) Degenerate states with $m = 1/2$ for $J_{\perp} = J_{\parallel}$ in a chain with open boundary conditions (OBCs) or periodic boundary conditions (PBCs). (b) Exact diagonalization results for a chain with $L = 14$ and $J_{\parallel} = 0.55$ with PBCs. Correlation functions $\langle \mathbf{S}_{l,i} \cdot \mathbf{S}_{m,j} \rangle$ between the spins at the same dimer ($l = m$), C_{\perp} , and neighbor dimers ($l = m + 1$), C_x or C_{\parallel} , as illustrated by the dashed ellipses. The estimated gapped regime in the thermodynamic limit is indicated.

chain due to an edge term in the Hamiltonian [29]. As also illustrated in Fig. 10(a), these triplets cause the presence of two neighboring dimers in a singlet state along the chain. This pair of singlets constitutes the edges of two domains, each of them having the alternation of one of the PBC ground states. Even in that case, $J_{\perp} = J_{\parallel}$, the ground state exhibits extensive degeneracy, since the energy does not change as we change the position of the pair of singlets. However, this degeneracy is lifted for $J_{\perp} \neq J_{\parallel}$. This domain wall or spinon carries spin $1/2$ and was studied in detail in Ref. [29]. At the magnetic field $h = h_0$ (see Fig. 2), one of the singlets in the domain wall pair changes to a triplet ($\uparrow\uparrow$), and the spin of the spinon changes from $-1/2$ to $+1/2$.

We use exact diagonalization for a chain with $L = 14$ dimers and PBCs to show in Fig. 10(b) the correlations

between the neighbor spins connected by each of the couplings: $J_{\perp} \equiv 1$, J_x , and $J_{\parallel} = 0.55$, which we call C_{\perp} , C_x , and C_{\parallel} , respectively, as functions of J_x . In particular, due to the twofold degeneracy for $J_{\perp} = J_{\parallel}$ [Fig. 10(a)], C_{\perp} is defined as the average of this correlation for two neighbor dimers. For $J_{\perp} = J_{\parallel}$, the singlet components are fixed, and so $C_{\perp} = -0.25$, since the dimer singlets are sided by two dimer triplets; $C_x = 0 = C_{\parallel}$. For $J_x < J_{\parallel}$, $C_x > 0$ and $C_{\parallel} < 0$, and thus there is a higher probability that the singlet component will fluctuate from the perpendicular direction to the parallel direction; in the case of $J_x > J_{\parallel}$ the roles of C_{\parallel} and C_x are exchanged in relation to the first case. However, we notice that the values of C_{\parallel} and C_x are not exactly exchanged about the $J_x = J_{\parallel}$ point, since $J_x \rightarrow 1 = J_{\perp}$ on the right side of the figure. In particular, C_x is lower than C_{\perp} for $J_x \gtrsim 0.97$.

In a short-range region of size $\sim \xi$, the spin correlations are similar to those of phase I, illustrated in Fig. 7, for $J_x < J_{\parallel}$ and similar to those of phase I' for $J_x > J_{\parallel}$. At the KT transition points, $\xi \rightarrow \infty$, and the correlations will exhibit a power-law behavior, as shown in Fig. 7. In the following, we estimate the critical points of the KT transitions.

Kosterlitz-Thouless transitions

In the Kosterlitz-Thouless transitions, the value of m is fixed at $1/2$, and the gap Δh closes following an essential singularity form. The asymptotic behavior of $\Gamma_{ij}(r)$ on the gapless side of the transition is given by Eq. (3) with $K = 1/2$, since the translation symmetry is broken and we have one boson for every two dimers [49] of the chain. A confident numerical technique to estimate the value of J_c from finite-size systems with open boundaries uses the exact expected value of K as $J \rightarrow J_c$. Within this methodology [37,51], the thermodynamic-limit value of K is estimated through an unbiased approach, as detailed below.

The transverse spin correlation functions of finite-size systems with open boundaries are calculated through Eq. (21). In Figs. 11(a) and 11(b), we present the typical behavior of $\Gamma_{11}(r)$ for two values of J_x and $m = 1/2$; see also Fig. 3. We must fit the data to the asymptotic form of the correlation, Eq. (3), to obtain K . However, in a system with open boundaries, the value of K thus obtained strongly depends on the interval of r chosen to make the fit. To overcome this problem [51], we arbitrarily define some intervals of r and extrapolate the finite-size values of K to the thermodynamic limit for each interval. In Figs. 11(c) and 11(d), we present this extrapolation for the same values of J_x used to calculate the correlations shown in Figs. 11(a) and 11(b). In the extrapolation, we use a linear scale function to fit the points of the two largest system sizes. Notice that the extrapolated values of K for the three r intervals are very similar and have little dispersion. The minimum and maximum values of K , K_{\min} , and K_{\max} , respectively, of the three intervals are used to define our thermodynamic-limit estimate as $K = (K_{\max} + K_{\min})/2$, with error $(K_{\max} - K_{\min})/2$.

In Fig. 12(a) we show K as a function of J_x near the KT transition in the region $J_x < J_{\parallel}$, while in Fig. 12(b) we show K near the transition in the region $J_x > J_{\parallel}$; see also Fig. 3. Through these data, we estimate the values

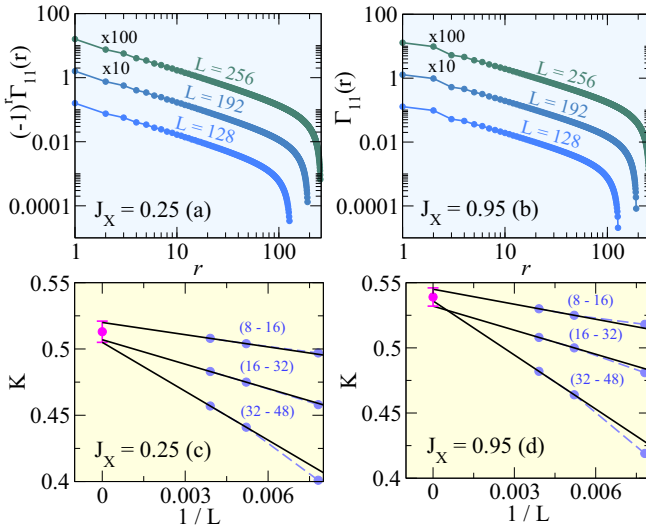


FIG. 11. Transverse spin correlation functions $\Gamma_{11}(r)$, where r is the distance along the chain, and Luttinger liquid exponent K for $m = 1/2$ and $J_{\parallel} = 0.55$. In (a), we present $(-1)^r \Gamma_{11}(r)$ for $J_{\times} = 0.25$, while in (b) we show $\Gamma_{11}(r)$ for $J_{\times} = 0.95$, in both cases for three system sizes: $L = 128, 192$, and 256 . In (c) and (d) we show the Luttinger liquid exponent as a function of $1/L$. K is calculated by fitting the correlations in (a) and (b) to the form $1/r^{1/2K}$ along the following intervals of r : $8 \leq r \leq 16$, $16 \leq r \leq 32$, and $32 \leq r \leq 48$, for (c) $J_{\times} = 0.25$ and (d) $J_{\times} = 0.95$. Extrapolating the values of K for each interval of r using a straight line through the two larger sizes, we obtain the minimum, K_{\min} , and maximum, K_{\max} , values of K for a given J_{\times} . The thermodynamic-limit value of K is defined as $(K_{\min} + K_{\max})/2$, and the error in K is defined as $(K_{\max} - K_{\min})/2$.

of J_{\times} for the two critical points as $J_{\times, \text{KT}_1} = 0.255 \pm 0.005$ and $J_{\times, \text{KT}_2} = 0.935 \pm 0.005$. To estimate the critical fields, we extrapolate to the thermodynamic limit the extreme fields, h_- and h_+ , of the magnetization steps for $m = 1/2$ in finite-size systems. We take h_- and h_+ for J_{\times} just before and just after J_c , considering the data shown in Figs. 12(a) and 12(b). We estimate the critical magnetic fields as $h_{\text{KT}_1} = 1.467 \pm 0.002$ and $h_{\text{KT}_2} = 1.98 \pm 0.01$ from the finite-size analysis shown in Figs. 12(c) and 12(d).

As was mentioned earlier, in the regime $J_{\perp} \gg (J_{\parallel}, J_{\times})$ and $h > 0$, in the first-order approximation [26,29], mappings onto the one-dimensional XXZ Heisenberg or spinless interacting fermion models are possible. Within these models, the Bethe ansatz solution allows one to locate precisely [26] the critical KT point at $J_{\times} = J_{\parallel}/3$, for $J_{\times} < J_{\parallel}$. In our case, $J_{\parallel} = 0.55$, and the value of the critical point is $J_{\times} = 0.18$ in the approximate approach, departing from our prediction, $J_{\times, \text{KT}_1} = 0.255 \pm 0.005$, by $\sim J_{\times, \text{KT}_1}^2$. For the second critical point, $J_{\times, \text{KT}_2} = 0.935 \pm 0.005$, the first-order approximation is not reliable since J_{\times} and J_{\parallel} have the same order of J_{\perp} .

VII. OTHER VALUES OF J_{\parallel} , AND CHANGING J_{\parallel} WITH J_{\times} CONSTANT

This section discusses the phase diagrams for $J_{\parallel} = 0.2$ and $J_{\parallel} = 0.8$, shown in Fig. 13, to grasp the stability of the features observed for $J_{\parallel} = 0.55$. We also analyze the phase diagrams

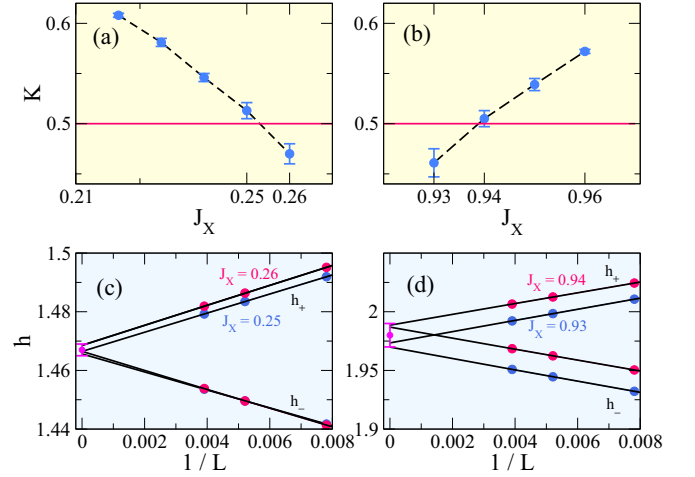


FIG. 12. (a) and (b) Thermodynamic-limit estimate for the Luttinger parameter K as a function of J_{\times} around the Kosterlitz-Thouless transition points. We estimate the critical points as $J_{\times, \text{KT}_1} = 0.255 \pm 0.005$ and $J_{\times, \text{KT}_2} = 0.935 \pm 0.005$. (c) and (d) Extrapolation of the critical values of the magnetic field h , h_- , and h_+ for $m = 1/2$ to the thermodynamic limit. We estimate $h_{\text{KT}_1} = 1.467 \pm 0.002$ and $h_{\text{KT}_2} = 1.98 \pm 0.01$.

for fixed J_{\times} , varying J_{\parallel} , and the KT transition points in the plane J_{\times} versus J_{\parallel} .

As expected in Fig. 5, the bicritical point and the first-order transition line are absent in the phase diagram for $J_{\parallel} = 0.2$ [Fig. 13(a)], since the minimum energy of the triplet and singlet bands does not cross for $J_{\parallel} < 0.5$. Furthermore, from Fig. 5, we can state that the bicritical point is located at $J_{\times} = 0.5$ and $h = 1 + 2J_{\parallel}$ for $J_{\parallel} > 0.5$, as exemplified by the phase diagram in Fig. 13(b), for $J_{\parallel} = 0.8$.

For $J_{\parallel} = 0.2$, there are only two first-order transition points, both at $J_{\times} = J_{\parallel} = 0.2$: one that separates the plateaus $m = 0$ and $m = 1/2$, and the other between the plateaus $m = 1/2$ and $m = 1$. However, as in the case of $J_{\parallel} = 0.55$, the closing of the plateau $m = 1/2$ on the two sides of the phase diagram, $J_{\times} < J_{\parallel}$ and $J_{\times} > J_{\parallel}$, follows a KT transition for $J_{\parallel} = 0.2$. The DMRG data show that the ground state is predominantly composed of a coherent superposition of the triplet component $|\uparrow\uparrow\rangle_l$ and $|s_l\rangle$, as in the cases $J_{\times} = 0.4$ and $J_{\parallel} = 0.55$ shown in Fig. 6.

The first-order transition points at $(J_{\times} = J_{\parallel} = 0.2, h = 1)$ and $(J_{\times} = J_{\parallel} = 0.2, h = h_{\text{FP}})$ are in the meeting of four second-order transition lines. At these points, there is the coexistence of the two disordered phases: $m = 0, m = 1/2$ in the first case and $m = 1/2, m = 1$ in the second. At these points, the critical magnetization states of the Luttinger liquid phases, $0 < m < 1/2$ for $h = 1$ and $1/2 < m < 1$ for $h = h_{\text{FP}}$, become equal to the disordered $m = 0$ or $m = 1/2$ phases and to the disordered $m = 1/2$ or $m = 1$ phases, respectively. We mention that a similar point is also observed at $(J_{\times} = J_{\parallel} = 0.55, h = 1)$ in the phase diagram of Fig. 3.

In Landau theory for thermal phase transitions [1,9], the *tetracritical* point is also found at the meeting of four second-order transition lines. In that case, there are three ordered phases with two distinct orders. In one of the phases, the “intermediate phase” [1,9], the two order parameters are finite,

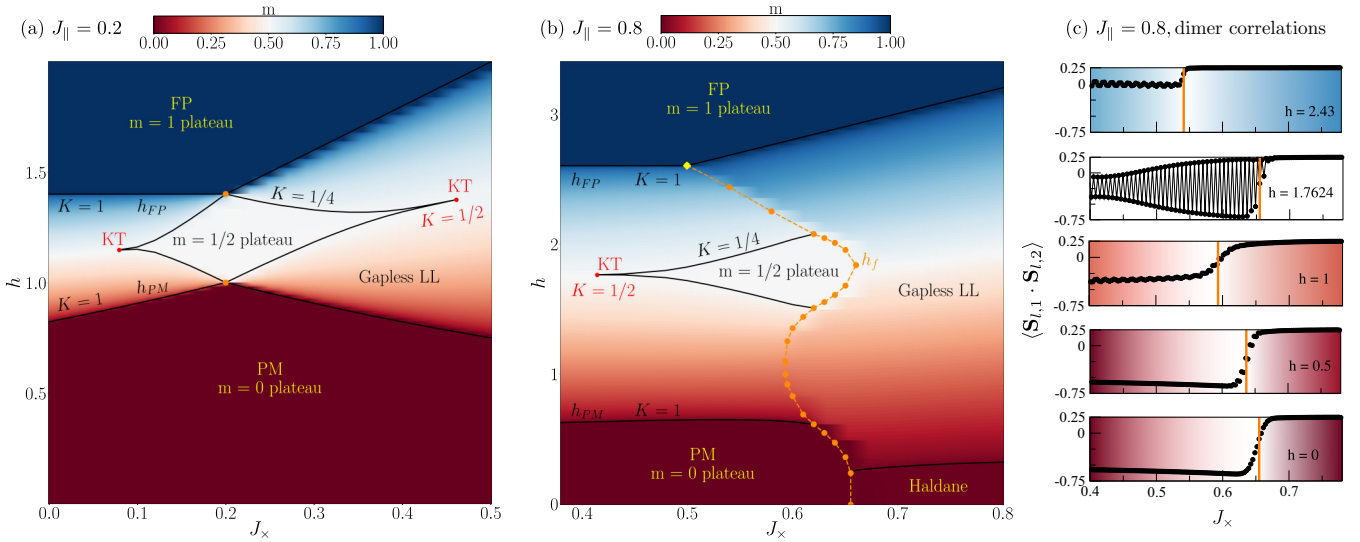


FIG. 13. DMRG results for the magnetic field h vs frustration J_x phase diagram for (a) $J_{\parallel} = 0.2$ and (b) $J_{\parallel} = 0.8$. The thermodynamic-limit transition lines are estimated from finite-size scale analysis of magnetization m as a function of h , while the color code for m for a system of size $L = 128$. In the phase diagrams, we highlight the fully polarized (FP) phase, the gapped paramagnetic (PM) phase, the gapless Luttinger liquid phases, and the value of the Luttinger liquid exponent K in the incommensurate transitions and the Kosterlitz-Thouless (KT) transition points. The dashed line in (b) is a first-order transition line, and the quantum bicritical point is indicated with a yellow diamond. We indicate the region at which the gapped singlet Haldane phase is observed. (c) J_x scans, for fixed h , of the intradimer correlation $\langle S_{l,1} \cdot S_{l,2} \rangle$. The vertical orange lines mark the first-order transition point in the thermodynamic limit, as shown in (b).

while in the other two phases, one or the other parameter is different from 0. The point $(J_x = J_{\parallel} = 0.2, h = 1)$ in the phase diagram of Fig. 13(a) could be a tetracritical point if one of the two phases $m = 0$ or $m = 1/2$ was critical or ordered, instead of disordered. A similar discussion can be had for the two similar first-order points mentioned: in $(J_x = J_{\parallel} = 0.2, h = 1)$ and $(J_x = J_{\parallel} = 0.55, h = 1)$.

The phase diagram is richer for $J_{\parallel} = 0.8$ [Fig. 13(b)]. In particular, we notice the presence of the bicritical point and the first-order transition line. The magnetization plateau, on the other hand, closes after a KT transition only in the region $J_x < J_{\parallel}$, in contrast to cases $J_{\parallel} = 0.2$ and 0.55 . The suppression of the KT transition point on the side $J_x > J_{\parallel}$ can be attributed to an increase in the downward slope of the critical field for the condensation of the singlet component, compared with the free hard-core boson model, due to an enhancement in the relevance of the interaction terms, compared with the case $J_{\parallel} = 0.55$. Although the transition lines in Fig. 13 have been estimated after a finite-size scaling analysis, we can have a vivid representation of the phases and their transitions by calculating the dimer correlations $\langle S_{l,1} \cdot S_{l,2} \rangle$ in a J_x scan, for fixed values of h [Fig. 13(c)]. In a J_x scan [52], we consider a ladder in which the value of J_x increases linearly from the left to the right side, such that it covers a given range of J_x , with a constant magnetic field h along the chain. In Fig. 13(c), we also marked with an orange line the estimated values of the thermodynamic-limit first-order transition points, as shown in the phase diagram for the respective values of h . We notice that $\langle S_{l,1} \cdot S_{l,2} \rangle = 0.25$ on the right side of the transition (phase II), while $\langle S_{l,1} \cdot S_{l,2} \rangle$ ranges from approximately -0.75 for $h = 0$ to approximately 0.0 for $h = 2.43$. Thus, on the right side of the first-order transition line, we observe an effective spin-1 chain. In particular, for $m = 0$, there is a gapped Haldane phase with a nontrivial topological ground

state, in contrast to the trivial gapped $m = 0$ state (PM) of the left side of the first-order transition line.

Changing J_{\parallel} with J_x fixed, and KT transition points

Due to the ladder symmetry under the exchange of J_x and J_{\parallel} , and of the label of the spins in odd (or even) dimers, the phase diagrams h versus J_{\parallel} for fixed $J_x = 0.55, 0.2$, and 0.8 exhibit the same transition lines shown in Figs. 3 and 13. In particular, the expressions for the critical FP field shown in Fig. 5 can be used to localize the bicritical point in the phase diagram h versus J_{\parallel} for fixed J_x . The bicritical point appears whenever there is a crossing between solutions h_c^e and h_c^t as we vary J_x or J_{\parallel} , with the second parameter constant. For fixed J_x , from Fig. 5, we can assert the absence of the bicritical point for $J_x < 0.5$, and we anticipate the presence of a bicritical point at $J_{\parallel} = 0.5$ and the field $h_c^e|_{J_{\parallel}=0.5} = h_c^t|_{J_{\parallel}=0.5} = 1 + 2J_x$, for $J_x > 0.5$.

We can also exploit the symmetry of the chain to obtain a more general behavior for the KT transition points as a function of J_x and J_{\parallel} . In Fig. 14, the calculated points for $J_{\parallel} = 0.2, 0.55$, and 0.8 , which were shown in Figs. 3 and 13, are supplemented by the corresponding symmetric points. We also show the prediction from perturbation theory [26]: $J_x = 3J_{\parallel}$ and $J_x = J_{\parallel}/3$ for comparison. The curves for KT_1 and KT_2 can be well fitted considering corrections J_{\parallel}^2 and J_{\parallel}^3 to the analytical expression of perturbation: $J_{\parallel}/3 + 0.16J_{\parallel}^2 + 0.12J_{\parallel}^3$ for KT_1 and $3J_{\parallel} - 3.77J_{\parallel}^2 + 2.60J_{\parallel}^3$ for KT_2 .

VIII. SUMMARY

We investigated the frustrated spin-1/2 ladder in a magnetic field h using DMRG and hard-core boson mapping. We have focused, in particular, on the quantum bicritical point,

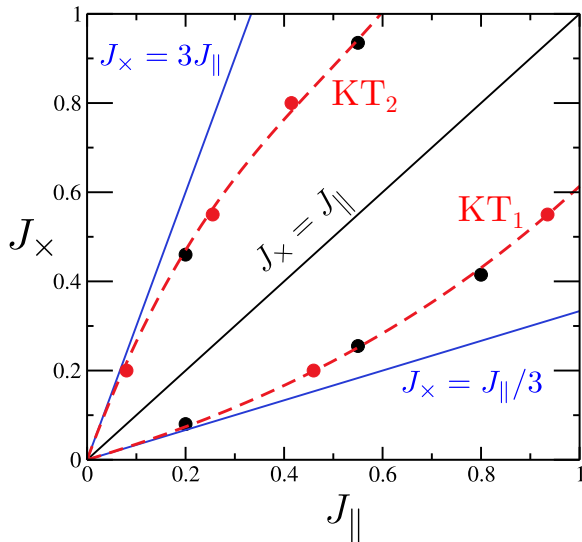


FIG. 14. The two lines of the KT transitions in the J_x vs J_{\parallel} plane: The points marked by black circles were calculated, while the points marked by red circles were drawn by exploiting the symmetry of the ladder. Error bars are less than or equal to the size of the symbols. The blue solid lines $J_x = 3J_{\parallel}$ and $J_x = J_{\parallel}/3$ are the results of perturbation theory. The dashed red curves are the best fittings to the numerical results of KT_1 and KT_2 : $J_{\parallel}/3 + 0.16J_{\parallel}^2 + 0.12J_{\parallel}^3$ and $3J_{\parallel} - 3.77J_{\parallel}^2 + 2.60J_{\parallel}^3$, respectively.

the first-order transition line, and the precise numerical determination of the Kosterlitz-Thouless transition points. We present numerical data from phase diagrams h versus J_x with $J_{\parallel} = 0.2, 0.55$, and 0.8 , but we use symmetry arguments and boson mapping to discuss phase diagrams h versus J_{\parallel} with J_x fixed.

The quantum bicritical point, which is the intersection of two second-order transition lines from the fully polarized phase to two distinct gapless phases, is observed at $(m = 1, J_x = 0.5)$ in the phase diagram h versus J_x for constant $J_{\parallel} > 0.5$, and at $(m = 1, J_{\parallel} = 0.5)$ for constant $J_x > 0.5$. The two competing gapless phases are characterized by the probability density for the occurrence of a singlet, $\langle n_s \rangle$, or a triplet with the rung state $S^z = 0$, $\langle n_0 \rangle$. With the help of these quantities, we have shown that one phase is composed of local singlets and $|\uparrow\uparrow\rangle$ triplets, while the other has only local triplets $|\uparrow\uparrow\rangle$ and triplets $|t_0\rangle$. In the last phase, the frustrated ladder is effectively described by a spin-1 chain in a magnetic field. In particular, the transverse spin correlation functions show that the total dimer spin has an antiferromagnetic quasi-long-range order in the direction perpendicular to the magnetic field in the phase rich in triplets $|t_0\rangle$. The transition from one gapless phase to the other is of the first-order kind in the field $h = h_f(J_x)$, and the magnetization curve as a function of the magnetic field exhibits a jump in the transition between them.

The first-order transition line $h_f(J_x)$ is observed in the phase diagram for $J_{\parallel} = 0.55$ and 0.8 and is absent for $J_{\parallel} = 0.2$. In fact, we argued that this line and the quantum bicritical point are not observed for $J_{\parallel} < 0.5$ or for $J_x < 0.5$ in the phase diagram h versus J_{\parallel} .

The $h = h_f(J_x)$ line starts at the quantum bicritical point, and to complete the whole physical picture, we have investigated the energy curves and phase coexistence along this line. Under a magnetic field $h = h_f$, the finite-size energy density curves exhibit two global minima corresponding to the magnetization states that bound the magnetization jump: $m_i^{(\text{jump})}$ and $m_f^{(\text{jump})}$, with unstable states between them. However, the scaling behavior of the energy density curves shows that the thermodynamic-limit curve is flat for magnetizations $m_i^{(\text{jump})} < m < m_f^{(\text{jump})}$ and thus is a stable equilibrium curve. In fact, we attribute to the interface between the two coexisting phases the departure $1/L$ of the finite-size energy curves from the stable thermodynamic-limit curve. By calculating the distribution of singlets and triplets $|t_0\rangle$ along the ladder, we were able to reveal that the states in the range $m_i^{(\text{jump})} < m < m_f^{(\text{jump})}$ are phase separated, and the two single-phase magnetizations ($m = m_i^{(\text{jump})}$ and $m = m_f^{(\text{jump})}$) coexist in distinct regions of the ladder. Following the magnitude of the magnetization jump, Δm , we have shown that $\Delta m \rightarrow 0$ as the bicritical point is approached along the line h_f .

We have made a precise estimation of the Kosterlitz-Thouless (KT) transition points associated with the closing of the fractional $m = 1/2$ plateau for $J_{\parallel} = 0.2, 0.55$, and 0.80 using the transverse spin correlation functions. For $J_{\parallel} = 0.2$ and 0.55 , there is one KT point on each side of the phase diagram, $J_x < J_{\parallel}$ and $J_x > J_{\parallel}$; for $J_{\parallel} = 0.8$, there is only one in the region $J_x < J_{\parallel}$. For $J_{\parallel} = 0.8$, the first-order transition line h_f crosses the plateau $m = 1/2$ so that there is a first-order transition from the plateau phase to the spin-1 phase. Finally, taking advantage of the ladder symmetry, we were able to estimate the curves of the KT points in the plane J_x versus J_{\parallel} .

We expect that our results will stimulate theoretical and experimental investigations in frustrated ladder systems, such as solid-state compounds or even correlated atoms in optical lattices, particularly focusing on the dynamical and thermal features associated with nonequilibrium states.

ACKNOWLEDGMENTS

We acknowledge the support from Coordenação de Aperfeiçoamento de Pessoal de Nível Superior (CAPES), Conselho Nacional de Desenvolvimento Científico e Tecnológico (CNPq), and Fundação de Amparo à Ciência e Tecnologia do Estado de Pernambuco (FACEPE), Brazilian agencies, including the PRONEX program, which is funded by CNPq and FACEPE, Grant No. APQ-0602-1.05/14.

- [1] P. Chaikin and T. Lubensky, *Principles of Condensed Matter Physics* (Cambridge University Press, Cambridge, 2000).
 [2] S. Sachdev, *Quantum Phase Transitions* (Cambridge University Press, Cambridge, 2011).

- [3] M. Continentino, *Quantum Scaling in Many-Body Systems: An Approach to Quantum Phase Transitions*, 2nd ed. (Cambridge University Press, Cambridge, 2017).

- [4] C. Lacroix, P. Mendels, and F. Mila, *Introduction to Frustrated Magnetism: Materials, Experiments, Theory*, Springer Series in Solid-State Sciences (Springer, Berlin, 2011).
- [5] M. Vojta, Frustration and quantum criticality, *Rep. Prog. Phys.* **81**, 064501 (2018).
- [6] J. L. Jiménez, S. P. G. Crone, E. Fogh, M. E. Zayed, R. Lortz, E. Pomjakushina, K. Conder, A. M. Läuchli, L. Weber, S. Wessel, A. Honecker, B. Normand, C. Rüegg, P. Corboz, H. M. Rønnow, and F. Mila, A quantum magnetic analogue to the critical point of water, *Nature (London)* **592**, 370 (2021).
- [7] J. Stapmanns, P. Corboz, F. Mila, A. Honecker, B. Normand, and S. Wessel, Thermal critical points and quantum critical end point in the frustrated bilayer Heisenberg antiferromagnet, *Phys. Rev. Lett.* **121**, 127201 (2018).
- [8] Y. Tokiwa, M. Garst, P. Gegenwart, S. L. Bud'ko, and P. C. Canfield, Quantum bicriticality in the heavy-fermion metamagnet YbAgGe, *Phys. Rev. Lett.* **111**, 116401 (2013).
- [9] M. E. Fisher and D. R. Nelson, Spin flop, supersolids, and bicritical and tetracritical points, *Phys. Rev. Lett.* **32**, 1350 (1974).
- [10] J. M. Kosterlitz, D. R. Nelson, and M. E. Fisher, Bicritical and tetracritical points in anisotropic antiferromagnetic systems, *Phys. Rev. B* **13**, 412 (1976).
- [11] C. Morice, P. Chandra, S. E. Rowley, G. Lonzarich, and S. S. Saxena, Hidden fluctuations close to a quantum bicritical point, *Phys. Rev. B* **96**, 245104 (2017).
- [12] N. Lopes, D. G. Barci, and M. A. Continentino, Finite temperature effects in quantum systems with competing scalar orders, *J. Phys.: Condens. Matter* **32**, 415601 (2020).
- [13] N. Lopes, M. A. Continentino, and D. G. Barci, One-loop effective potential for two-dimensional competing scalar order parameters, *Phys. Lett. A* **384**, 126095 (2020).
- [14] E. Dagotto, Experiments on ladders reveal a complex interplay between a spin-gapped normal state and superconductivity, *Rep. Prog. Phys.* **62**, 1525 (1999).
- [15] S. R. White, R. M. Noack, and D. J. Scalapino, Resonating valence bond theory of coupled Heisenberg chains, *Phys. Rev. Lett.* **73**, 886 (1994).
- [16] T. Giamarchi, *Quantum Physics in One Dimension* (Clarendon, Oxford, 2004).
- [17] R. Chitra and T. Giamarchi, Critical properties of gapped spin-chains and ladders in a magnetic field, *Phys. Rev. B* **55**, 5816 (1997).
- [18] T. Giamarchi and A. M. Tsvelik, Coupled ladders in a magnetic field, *Phys. Rev. B* **59**, 11398 (1999).
- [19] T. Hikihara and A. Furusaki, Spin correlations in the two-leg antiferromagnetic ladder in a magnetic field, *Phys. Rev. B* **63**, 134438 (2001).
- [20] C. Rüegg, K. Kiefer, B. Thielemann, D. F. McMorrow, V. Zapf, B. Normand, M. B. Zvonarev, P. Bouillot, C. Kollath, T. Giamarchi, S. Capponi, D. Poilblanc, D. Biner, and K. W. Krämer, Thermodynamics of the spin Luttinger liquid in a model ladder material, *Phys. Rev. Lett.* **101**, 247202 (2008).
- [21] M. Klanjšek, H. Mayaffre, C. Berthier, M. Horvatić, B. Chiari, O. Piovesana, P. Bouillot, C. Kollath, E. Orignac, R. Citro, and T. Giamarchi, Controlling Luttinger liquid physics in spin ladders under a magnetic field, *Phys. Rev. Lett.* **101**, 137207 (2008).
- [22] B. Thielemann, C. Rüegg, H. M. Rønnow, A. M. Läuchli, J.-S. Caux, B. Normand, D. Biner, K. W. Krämer, H.-U. Güdel, J. Stahn, K. Habicht, K. Kiefer, M. Boehm, D. F. McMorrow, and J. Mesot, Direct observation of magnon fractionalization in the quantum spin ladder, *Phys. Rev. Lett.* **102**, 107204 (2009).
- [23] M. P. Gelfand, Linked-tetrahedra spin chain: Exact ground state and excitations, *Phys. Rev. B* **43**, 8644 (1991).
- [24] S. R. White, Equivalence of the antiferromagnetic Heisenberg ladder to a single $S=1$ chain, *Phys. Rev. B* **53**, 52 (1996).
- [25] A. Honecker, F. Mila, and M. Troyer, Magnetization plateaus and jumps in a class of frustrated ladders: A simple route to a complex behaviour, *Eur. Phys. J. B* **15**, 227 (2000).
- [26] F. Mila, Ladders in a magnetic field: A strong coupling approach, *Eur. Phys. J. B* **6**, 201 (1998).
- [27] T. Tonegawa, T. Nishida, and M. Kaburagi, Ground-state magnetization curve of a generalized spin-1/2 ladder, *Phys. B (Amsterdam)* **246-247**, 368 (1998).
- [28] K. Totsuka, Magnetization plateau in the $S = \frac{1}{2}$ Heisenberg spin chain with next-nearest-neighbor and alternating nearest-neighbor interactions, *Phys. Rev. B* **57**, 3454 (1998).
- [29] J.-B. Fouet, F. Mila, D. Clarke, H. Youk, O. Tchernyshyov, P. Fendley, and R. M. Noack, Condensation of magnons and spinons in a frustrated ladder, *Phys. Rev. B* **73**, 214405 (2006).
- [30] K. Penc, J.-B. Fouet, S. Miyahara, O. Tchernyshyov, and F. Mila, Ising phases of Heisenberg ladders in a magnetic field, *Phys. Rev. Lett.* **99**, 117201 (2007).
- [31] F. Michaud, T. Coletta, S. R. Manmana, J.-D. Picon, and F. Mila, Frustration-induced plateaus in $S \geq \frac{1}{2}$ Heisenberg spin ladders, *Phys. Rev. B* **81**, 014407 (2010).
- [32] J. M. Kosterlitz, Nobel Lecture: Topological defects and phase transitions, *Rev. Mod. Phys.* **89**, 040501 (2017).
- [33] J. M. Kosterlitz and D. J. Thouless, Ordering, metastability and phase transitions in two-dimensional systems, *J. Phys. C: Solid State Phys.* **6**, 1181 (1973).
- [34] J. C. Xavier, R. G. Pereira, M. E. S. Nunes, and J. A. Plascak, Coexistence of spontaneous dimerization and magnetic order in a transverse-field Ising ladder with four-spin interactions, *Phys. Rev. B* **105**, 024430 (2022).
- [35] M. Nayak, D. Blosser, A. Zheludev, and F. Mila, Magnetic-field-induced bound states in spin- $\frac{1}{2}$ ladders, *Phys. Rev. Lett.* **124**, 087203 (2020).
- [36] A. M. do Nascimento-Junior and R. R. Montenegro-Filho, Magnetic phase separation in a frustrated ferrimagnetic chain under a magnetic field, *Phys. Rev. B* **99**, 064404 (2019).
- [37] R. R. Montenegro-Filho, F. S. Matias, and M. D. Coutinho-Filho, Topology of many-body edge and extended quantum states in an open spin chain: $1/3$ plateau, Kosterlitz-Thouless transition, and Luttinger liquid, *Phys. Rev. B* **102**, 035137 (2020).
- [38] L. M. Veríssimo, M. S. S. Pereira, J. Strečka, and M. L. Lyra, Kosterlitz-Thouless and Gaussian criticalities in a mixed spin- $(\frac{1}{2}, \frac{5}{2}, \frac{1}{2})$ Heisenberg branched chain with exchange anisotropy, *Phys. Rev. B* **99**, 134408 (2019).
- [39] K. Karl'ová, J. Strečka, and M. L. Lyra, Breakdown of intermediate one-half magnetization plateau of spin-1/2 Ising-Heisenberg and Heisenberg branched chains at triple and Kosterlitz-Thouless critical points, *Phys. Rev. E* **100**, 042127 (2019).
- [40] T. Sakai and S. Yamamoto, Critical behavior of anisotropic Heisenberg mixed-spin chains in a field, *Phys. Rev. B* **60**, 4053 (1999).
- [41] U. Schollwöck, The density-matrix renormalization group, *Rev. Mod. Phys.* **77**, 259 (2005).

- [42] S. R. White, Density matrix formulation for quantum renormalization groups, *Phys. Rev. Lett.* **69**, 2863 (1992).
- [43] S. R. White, Density-matrix algorithms for quantum renormalization groups, *Phys. Rev. B* **48**, 10345 (1993).
- [44] F. Gebhard, K. Bauerbach, and Ö. Legeza, Accurate localization of Kosterlitz-Thouless-type quantum phase transitions for one-dimensional spinless fermions, *Phys. Rev. B* **106**, 205133 (2022).
- [45] S. Wessel, B. Normand, F. Mila, and A. Honecker, Efficient quantum Monte Carlo simulations of highly frustrated magnets: The frustrated spin-1/2 ladder, *SciPost Phys.* **3**, 005 (2017).
- [46] B. Bauer, L. D. Carr, H. G. Evertz, A. Feiguin, J. Freire, S. Fuchs, L. Gamper, J. Gukelberger, E. Gull, S. Guertler, A. Hehn, R. Igarashi, S. V. Isakov, D. Koop, P. N. Ma, P. Mates, H. Matsuo, O. Parcollet, G. Pawłowski, J. D. Picon *et al.*, The ALPS project release 2.0: Open source software for strongly correlated systems, *J. Stat. Mech.: Theory Exp.* (2011) P05001.
- [47] M. Fishman, S. R. White, and E. M. Stoudenmire, The ITensor software library for tensor network calculations, *SciPost Phys. Codebases* **4** (2022).
- [48] M. Oshikawa, M. Yamanaka, and I. Affleck, Magnetization plateaus in spin chains: “Haldane gap” for half-integer spins, *Phys. Rev. Lett.* **78**, 1984 (1997).
- [49] M. A. Cazalilla, R. Citro, T. Giamarchi, E. Orignac, and M. Rigol, One dimensional bosons: From condensed matter systems to ultracold gases, *Rev. Mod. Phys.* **83**, 1405 (2011).
- [50] V. Zapf, M. Jaime, and C. D. Batista, Bose-Einstein condensation in quantum magnets, *Rev. Mod. Phys.* **86**, 563 (2014).
- [51] T. D. Kühner, S. R. White, and H. Monien, One-dimensional Bose-Hubbard model with nearest-neighbor interaction, *Phys. Rev. B* **61**, 12474 (2000).
- [52] S. Jiang, J. Romhányi, S. R. White, M. Zhitomirsky, and A. Chernyshev, Where is the quantum spin nematic? *Phys. Rev. Lett.* **130**, 116701 (2023), and references therein.